

## Mass Modeling of NEP Power Conversion Concepts for Human Mars Exploration

William Machemer<sup>1</sup>, Matthew Duchek<sup>1</sup>, Christopher Harnack<sup>1</sup>, Emanuel Grella<sup>1</sup>, Dennis Nikitaev<sup>2</sup>, and Corey D. Smith<sup>2</sup>

<sup>1</sup>Advanced Projects Denver, Analytical Mechanics Associates, Denver, CO, 80211

<sup>2</sup>Advanced Projects Huntsville, Analytical Mechanics Associates, Huntsville, AL, 35806

Primary Author Contact Information: 720-648-3986, william.machemer@ama-inc.com

DOI: #####

*The specific mass (mass per unit of electric power output) of an NEP power conversion system is an important metric for the performance and feasibility of a crewed NEP vehicle. This work explores a component level buildup of the specific mass for a crewed NEP vehicle. The buildup is highly parametric and avoids being tied to specific technologies where practical. This allows the specific mass to be calculated for a variety of assumptions and operating conditions and be used to optimize particular design variables or compare different system configurations. The values of specific mass are dependent on assumptions with significant uncertainty; comparison between cases and trends observed in the models are the main goal of the work presented here. To demonstrate the level of insight this type of modeling can provide, the impacts of compressor inlet temperature, turbine inlet temperature, and radiator pressure drop on specific mass are explored. In addition, the specific mass can be used to assess the benefit of separating the radiator and reactor loop from the power conversion cycle.*

### I. INTRODUCTION

The two primary technologies under consideration by NASA for crewed missions to Mars are Nuclear Thermal Propulsion (NTP) and Nuclear Electric Propulsion (NEP).<sup>1</sup> The former uses a reactor to heat propellant and accelerate it out of a nozzle while the latter converts the nuclear thermal power to electricity through a power conversion cycle such as a Brayton or Rankine cycle.<sup>1</sup> The electrical power is used by electric propulsion devices such as Hall or magnetoplasmadynamic (MPD) thrusters. To down-select between the two options, parameters such as reliability, performance, technology readiness level (TRL), and system mass must be compared. Within the NEP down-selection there are technology and system design decisions that will affect the system's mass such as: single versus triple loop configurations, turbine inlet temperature, compressor inlet temperature, power level, and others. This work will explore how technology and design decisions will affect the total mass of an NEP power conversion system. The observed trends can then be used to inform technology maturation plans.

The mass model presented in this work is one of three models developed by Analytical Mechanics Associates.<sup>2</sup>

These models have been integrated together to analyze the NEP trade space. In addition to the mass model, a performance model solves the Brayton cycle thermodynamics<sup>3</sup> and a mission model looks at the  $\Delta V$  and time requirements for an opposition-class trajectory.<sup>4</sup> The goal of these models is to illustrate the trends in specific mass and allocate mass goals to subsystems for technology development. The conclusions and general trends outlined in this work are not expected to change; however, the presented values are subject to change as the ongoing technology maturation effort provides more realistic assumptions and hardware to validate against.

One of the most important trades when designing an NEP power conversion system is the configuration of the power conversion cycle. A single loop configuration consists of a single working fluid, He-Xe in this analysis, running through the Brayton cycle, reactor, and radiator. In the triple loop configuration, the reactor, radiator, and Brayton cycle are given individual loops and working fluids that interact through heat exchangers (HX). These separate loops require additional components, such as pumps and accumulators, but allow for more compact reactor and radiator design, due to the use of liquid metals as the secondary and tertiary fluids. In this analysis, the radiator loop uses sodium potassium (NaK), while the reactor uses Lithium (Li) as its working fluid. The Brayton cycle is also assumed to be separated into four Brayton converters operating in parallel and each outputting one fourth of the total electrical power output.

The NEP system is made up of 5 critical technology elements (CTEs) shown in Fig. 1: the reactor system (RXS), power conversion system (PCS), power management and distribution (PMAD), electric propulsion system (EPS), and primary heat rejection system (PHRS). The power system specific mass,  $\alpha_{ps}$ , is defined as the mass of RXS, PCS, PMAD and PHRS, in kg, per kilowatt of electrical power output to the EPS. The largest components in each of these CTEs are modeled individually; based on either a first principles physics-based approach, published relations, or point designs scaled up and down. Notional geometries have been established for the ducting, turboalternator, reactor, and radiator. Where possible the component mass models were verified with comparisons to benchmark cases.

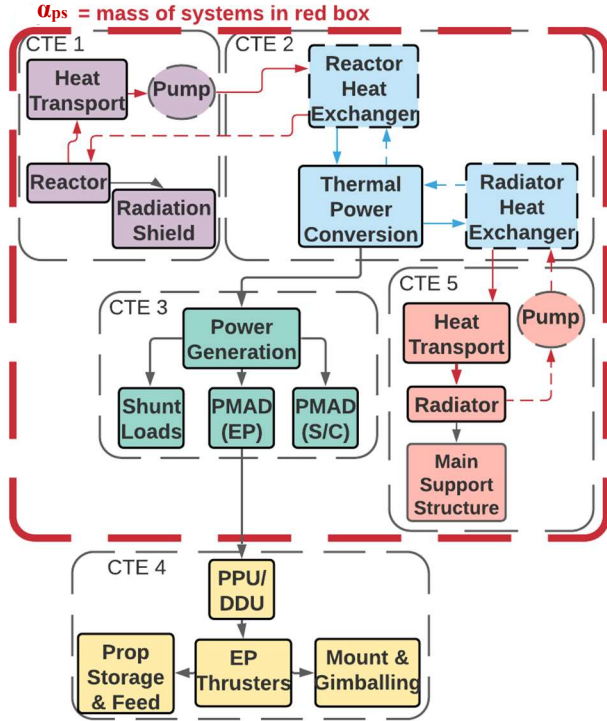


Fig. 1. Critical technology elements (CTEs).

## II. PERFORMANCE MODEL RESULTS

The mass model works in conjunction with the performance model, which solves the power conversion cycles thermodynamics.<sup>3</sup> The performance model will calculate the cycle efficiency, mass flow rate, radiator area, and cycle state points for a variety of operating conditions. These values are then used to estimate the mass for the NEP system components. Some of the important assumptions in the performance model are listed in TABLE I. Electric power level and turbine inlet temperature as user inputs with two values each considered in this paper.

TABLE I. Performance model assumptions which also effect results of the mass model.

Model Parameter	Assumption
Electric power level	2 MW <sub>e</sub> , 4 MW <sub>e</sub>
Turbine inlet temperature	1200 K, 1400K
He-Xe ratio	72 wt% He
Turbine inlet pressure	2 MPa
Turbine efficiency	0.89
Compressor efficiency	0.85
Radiator emissivity	0.9
Radiator view factor	0.85
Radiator sink temperature	4 K
Recuperator effectiveness	0.9
Reactor HX effectiveness	0.9
Radiator HX effectiveness	0.9
Compressor inlet temperature	Optimized
Radiator pressure drop	Optimized

Parameters such as the turbine and compressor efficiencies have a significant impact on the cycle efficiency, required radiator area and system mass. These assumptions are held constant in this analysis, and it should be noted that there is uncertainty in their values due to the low TRL of the components. The alpha predictions given in Section IV are highly dependent on the assumptions chosen. Variables like the compressor inlet temperature or the radiator pressure drop have a significant effect on both the mass and performance of an NEP system. To optimize these variables, both the performance and mass models must be used in conjunction.

## III. COMPONENT MASS MODEL FORMULATIONS

### III.A. Reactor

#### III.A.1. Reactor

To model the mass constituents of the reactor assembly, an algorithm has been developed to converge on reactor geometry to reach desired state points of the Brayton cycle. The reactor sizing model utilizes a coupled thermal hydraulic, neutronic (using the SERPENT tool), and mass approach for various unit cell geometry options. The model varies the radial dimensions and thermal power density to reach a desired reactor outlet temperature. To simplify the power conversion system models, thousands of test cases at various Brayton operating conditions (e.g., mass flow rate, temperature, pressure) have been simulated to output the reactor mass and pressure drop. These data points are interpolated using high-fidelity, multi-dimensional spline fits.

The reactor sizing model starts with a precalculated mass for each unit cell based on material-specific volume calculations and room temperature densities. The total active core mass is obtained by multiplying the per unit cell mass by the required number of unit cells to reach the desired reactor outlet temperature. The active core is surrounded by a constant thickness radial and axial reflector to parametrically mimic reactor point designs. The model also includes sizing of the external pressure vessel based on the inlet fluid pressure, using the hoop stress Eq. (1); where P is the maximum pressure, r is the radius and t is the thickness.

$$\sigma_y = \frac{Pr}{t} \quad (1)$$

The radius and length of the pressure vessel scale proportionally with the converged values from the thermal hydraulic sizing. Ultimate material strengths of various pressure vessel options are used to calculate the required annular thickness. Finalized geometry is used to calculate total volume and mass using material-specific density. Masses of several additional subcomponents, as seen in TABLE II, are calculated using RSMAS-D correlations

which are based on the SP-100 project reactor concepts.<sup>5</sup> While SP-100 focused on pumped Li reactors, the model is assumed to be valid for both He-Xe gas-cooled and pumped liquid Li options due to the comparatively small mass constituents of the reactor subcomponents.

**TABLE II.** Mass constituents obtained from the reactor sizing approach and RSMASS-D scaling correlations.

From Reactor Sizing Model	From RSMASS-D Correlations
Active core (fuel, moderator, cladding)	Instrumentation and control (I&C)
Axial and radial reflector	Safety systems
Pressure vessel	Structural support
	Nose cone, other externals

### III.A.2. Shield

To minimize radiation damage to the power conversion system, radiator, and crewed habitat, the external shield is composed of attenuative materials to reduce the gamma and neutron intensity. The largest contributor to the external shield mass is the gamma shield thickness. While typically thin in comparison to the other material layers, the gamma shield requires heavy elements, such as refractory metals or depleted uranium, which drastically increases the mass. Light elements tend to be neutron attenuators and are commonly found in low density materials, such as lithium hydride or boron carbide. Two layers of tungsten were used for the gamma shield material at 6 cm thick and two layers of lithium hydride for the neutron shield at 10 cm thick. These values were picked from assumptions made in RSMASS-D models developed by Sandia National Laboratories.<sup>5</sup>

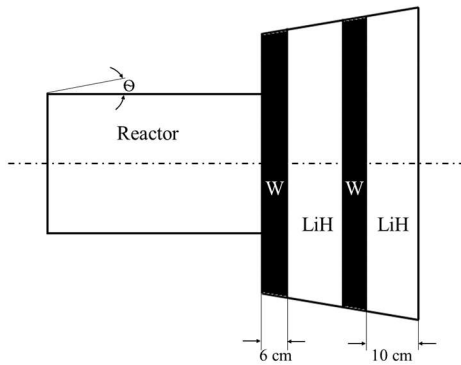


**Fig. 2.** Reactor external shield geometry.

The geometry of the shield radii will vary based on the converged reactor length and diameter. The assumed geometry can be seen in Fig. 2 and it is based on geometry from Sandia National Laboratories.<sup>5</sup> Acceptable levels of radiation are reached using a shadow shield with a reference angle representative of the angle between the reactor and the radiator paneling, assumed to be 10° in this case.

### III.A.3. Ducting, Pump, and Accumulator

For the triple loop configuration, additional ducting, a pump, and an accumulator must be accounted for. The ducting diameter is sized to accommodate the mass flow through the reactor loop with a 1% pressure drop along its length according to Eq. (2) (Ref. 6); where  $f$  is the friction factor,  $\rho$  is the fluid density,  $L$  is the pipe length,  $d$  is the pipe diameter, and  $u$  is the fluid velocity. The thickness of the pipe is then determined using hoop stress, Eq. (1). The pipe material is assumed to be titanium and have a factor of safety of 2 against yielding.

$$\Delta P = f \rho \left( \frac{L}{d} \right) \left( \frac{u^2}{2} \right) \quad (2)$$

The length of ducting was approximated as 4 meters using SolidWorks to layout a conceptual system design of the power conversion system as seen in Fig. 3. The ducting to the reactor is accounted for in the Brayton cycle ducting (Section III.D) for the single loop configuration. The pump mass was scaled off the specific mass, 250 kg per kW of required pump power, of liquid metal pumps from information gathered at the NEP Thermal Management Technical Interchange Meeting.<sup>7</sup> This results in a very conservative estimate of the pump mass, which can be expected to go down significantly with future technology development in this area. The accumulator mass was scaled using the volume differential in the reactor loop fluid at rest and operational temperature. The basis for this scaling was the Li accumulator design from Tournier and El-Genk.<sup>8</sup>

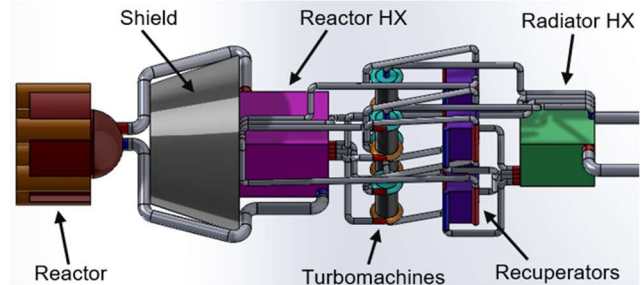


**Fig. 3.** Conceptual SolidWorks layout of NEP power conversion system.

### III.B. Turboalternator

The turboalternator mass model is anchored by the turboalternator used in the Brayton Rotating Unit (BRU), developed in the 1970s by NASA (Ref. 9). The BRU was broken into four mass allocations to find the total mass: turbine & compressor rotors, shaft, inlet & outlet scrolls, bearings, main frame, alternator housing, & alternator.

The component sizes scale with the rotor diameters and inlet and outlet pressure. Those inputs came from a Brayton cycle turbomachinery model based on the specific speed and specific diameter discussed in Nikitaev.<sup>10</sup> The relative size between the rotors and all other components were determined from drawings of the BRU. For example,

the shaft connecting the rotors gets longer and thicker if the rotors diameter increases.

The rotors, shaft, and scroll shapes were simplified for easier mass calculations. The rotors shape was assumed to be a short cylinder with a conical frustum on top and a hole for the shaft through the center. The inlet and outlet scrolls were simplified to a torus shape with a thickness that scales with pressure. The hoop stress, Eq (1) and a FOS of 1.5 were used. Inconel 718 was assumed material to calculate the mass of all components. The bearings, main frame, alternator housing, & alternator were included as a multiplication factor of the mass of all other components. The multiplication factor to match BRU was found to be 3.34. A comparison between the known BRU masses and the model's output is seen below in TABLE III.

**TABLE III.** Turboalternator mass build up and validation.

Component	BRU Mass (kg)	Predicted Mass (kg)	% Diff.
Turbine Rotor	N/A	1.79	N/A
Compressor Rotor	N/A	1.10	N/A
Shaft	9.89	9.89	~0.00%
Scrolls	N/A	6.67	N/A
Mainframe, etc.	N/A	45.5	N/A
Total mass	65.0	65.0	~0.00%

For this modeling effort the turboalternator mass model was simplified to be dependent solely on electrical power. To do this, the Brayton cycle turbomachinery model developed in Nikitaev<sup>10</sup> was swept through a power range of 100 – 5000 kW<sub>e</sub> in 100 kW<sub>e</sub> increments. Using this output, an  $\alpha$  for each point was calculated. MATLAB's Curve Fitting Toolbox was used to develop a curve fit, see Eq. (3), for  $\alpha$  as a function of electrical power, in kW<sub>e</sub>. The R<sup>2</sup> value was greater than 0.97. It is important to note that the turbine inlet temperature and pressure were set to 1150 K and 1.35 MPa when the power range swept through. The relationship would be different for other temperatures and pressures but gives an adequate approximation for this analysis.

$$\alpha_{Turbo,He-Xe} = 1.37Power^{-0.2196} \quad (3)$$

### III.C. Heat Exchangers

The mass of the recuperator was generated by scaling prior work based on the mass flow rate, pressure, and effectiveness. The model was also extended to the heat exchangers that interface with the secondary and tertiary loops. Jupiter Icy Moons Orbiter (JIMO) (Ref. 11) and the Solar Dynamic Brayton for Space Station Freedom (SDB SSF) (Ref. 12) projects were used as references for this model because both studies listed detailed information on the recuperator and radiator heat exchanger used:

**TABLE IV:** Heat exchanger (HX) values from JIMO (Ref. 11) and SDB SSF (Ref. 12)

	JIMO	SDB SSF
Mass flow rate Brayton	3.73 kg/s	1.15 kg/s
Volume recuperator	0.7 m <sup>3</sup>	0.3 m <sup>3</sup>
High pressure into recuperator	1.38 MPa	0.543 MPa
Mass of the recuperator	486 kg	162 kg
Mass flow rate radiator HX	2.59 kg/s	0.37 kg/s
Volume radiator HX	0.2 m <sup>3</sup>	0.08 m <sup>3</sup>
High pressure into radiator HX	0.7 MPa	2.96 MPa
Mass of the radiator HX	355 kg	85 kg

The density of the heat exchanger was assumed to scale linearly with the pressure, representing the thickness of the tubes needed. The highest pressure into the heat exchanger was used for this calculation. The volume of the heat exchanger was assumed to scale linearly with the mass flow rate, representing the number of tubes needed to accommodate the flow. No references could be found to anchor the reactor heat exchanger; however, it has enough commonality to the radiator heat exchanger to allow the same scaling relationship to be used. The scaling for the reactor heat exchanger used the radiator heat exchanger values from TABLE IV with multiplication factors to account for the higher temperature environment. The density of the reactor heat exchanger was assumed to be 0.75 that of the gas cooler based on the relative strength of some high temperature materials. The volume was also assumed to be 1.5 times larger for the reactor heat exchanger. These assumptions are based on Sunden's<sup>13</sup> overview of the design considerations for high temperature heat exchangers given. Sunden also supplies a chart for recuperator specific volume as a function of effectiveness,  $\epsilon$ , from which the following curve fit was developed:

$$SV = 8.1E - 5 * \exp(15.8 * \epsilon) \quad (4)$$

The specific volume, SV, has units of cm<sup>3</sup>/(kg\*s). Both JIMO and the Solar Dynamic Brayton assume an efficiency of 0.95. Eq. (4). This equation was used to scale the specific volume as a function of the effectiveness as well as pressure and mass flow as described above.

### III.D. Brayton Cycle Ducting

The Brayton cycle ducting is also titanium and was sized in the same way as the reactor ducting, using Eqs. (1) and (2) but assuming a 2% loss pressure along its length. The approximate length of the Brayton cycle ducting, based on the SolidWorks model in Fig. 3, is 7 meters for the triple loop configuration and 11 for the single loop configuration (including the ducting to the reactor).

### III.E. Heat Rejection

Work done by Siamidis<sup>14</sup> provided a starting point for the radiator mass model, however, this model needed to be generalized to be applicable to any radiator size and mass flow rate. The general radiator geometry and configuration, shown in Fig. 4, were based off Siamidis' model. Four of these 'wings' were oriented 90° from each other. For larger areas, additional booms were added to the right with increasing numbers of panels. The ducting is assumed to go through the 'wings' mostly in series, serving no more than 4 panels in parallel. Each 'wing' is assumed to be a parallel loop. For some high-power systems, the mass flow rate through the radiator becomes too large and requires impractical pipe diameters to plumb each 'wing' in series. Therefore, when the mass flow rate is greater than 30 kg/s each wing must be split into multiple parallel loops.

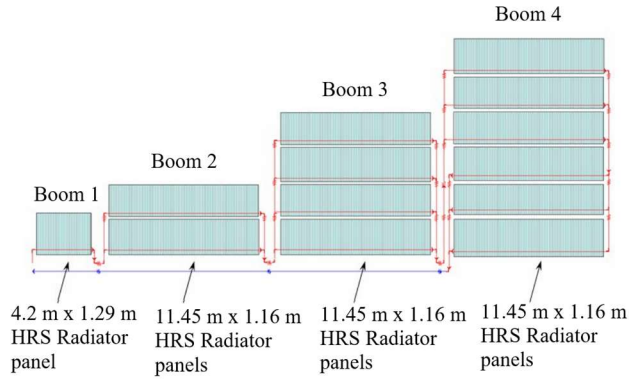


**Fig. 4.** Siamidis radiation configuration<sup>14</sup>

#### III.E.1. Ducting

The diameter and thickness of the ducting is calculated in the same way as the Brayton cycle and reactor loop ducting, assuming titanium as the material and using Eqs. (1) and (2). The primary difference being that the pressure drop across the radiator is much larger and treated as an independent variable that can be optimized. These relationships result in the pipe mass being inversely proportional to the pressure drop. This means that a lighter radiator can be bought by increasing the pressure drop and vice versa.

#### III.E.2. Panels

The heat pipes are assumed to be perpendicular to the pumped fluid loop and run the length of the panels. The heat pipes are placed every 10 cm and have an inner diameter of 1.25 cm and a thickness of 0.7 mm. The heat pipes are titanium with a water working fluid and liquid fill fraction of 10%. The heat pipes are assumed to be isothermal at the same temperature as the working fluid in the pumped loop, while the carbon fiber panels are assumed to have a temperature loss away from the heat pipe. To account for this a 10 % margin was added to the radiator area calculated in the performance model (assuming there

was no temperature loss between the loop fluid and the radiating surface). Given these assumptions, a panel thickness can be calculated using Eqs. (5), (6), (7), and (8), derived in Chang.<sup>15</sup>

$$\zeta = 2 \left[ \sigma_{SB} \epsilon T_{avg}^3 \left( \frac{s}{2} \right)^2 F \right] / [k t_{panels}] \quad (5)$$

$$\eta = (1 - 1.2491\zeta + 1.0093\zeta^2)(1 - \theta^4), \quad 0.01 \leq \zeta \leq 0.2 \quad (6)$$

$$\eta = (-0.4049 \log(\zeta) + 0.5321)(1 - \theta^4), \quad 0.2 \leq \zeta \leq 2.0$$

$$\theta = \frac{T_{sink}}{T_{avg}} \quad (7)$$

$$\eta = \frac{Q_{fin,real}}{Q_{fin,perfect}} \quad (8)$$

Terms are defined as follows:  $\zeta$  is a non-dimensional number related to fin geometry,  $\sigma_{SB}$  is the Stefan-Boltzmann constant,  $\epsilon$  is the emissivity,  $T_{avg}$  is the average radiating temperature,  $s$  is the heat pipe spacing,  $F$  is the view factor,  $k$  is the thermal conductivity of the panel material,  $t_{panels}$  is the thickness of the panels,  $\eta$  is the fin efficiency,  $T_{sink}$  is the temperature of deep space (4 K),  $Q_{fin,real}$  is the heat rejection requirement calculated from the performance model,  $Q_{fin,perfect}$  is the heat that could be rejected without any temperature loss in the panels (in this case 10% higher than the heat rejection requirements). The ducting and panel masses were verified against the results obtained by Siamidis and yielded a percent difference of less than 5%. Verification of this model at the higher power levels of a crewed Mars missions is much more difficult due to lack of prior work and hardware development.

#### III.E.3. Structure

The support structure for both radiator models is scaled from FEA work done on the central truss by the NASA Advanced Concepts Office (ACO) and Aerojet.<sup>16</sup> They estimated a truss mass of 4,000 kg for a 2,500 m<sup>2</sup> radiator. The truss mass was assumed to scale linearly with radiator area, giving the truss mass of 1.6 kg per m<sup>2</sup> of radiator.

#### III.E.4. Pump and Accumulator

The pump masses also need to be accounted for in the triple loop configuration. As with the reactor loop, pump mass was estimated from information gathered at the NEP Thermal Management Technical Interchange Meeting<sup>7</sup> and the accumulator mass was estimated using Tournier and El-Genk.<sup>8</sup> The pump mass was scaled using a specific mass of 250 kg per kW of required pump power, which provides an upper bound on the mass of the pump. Future work and technology maturation for liquid metal pumps will significantly reduce the uncertainty in the pump mass estimates. The accumulator mass was scaled using the

volume differential in the radiator loop fluid at rest and operational temperature.

### III.F. Power Management and Distribution (PMAD)

The PMAD  $\alpha$  model was developed in a study of mission sensitivities in high-power electric propulsion systems.<sup>17</sup> A scaling equation was developed from the  $\alpha$  versus  $kW_e$  plot provided in this study:

$$\alpha_{PMAD} = 128.63 Power^{-0.502} \quad (9)$$

Two additional components are accounted for in the PMAD  $\alpha$ : a PMAD radiator and parasitic load radiator. The former discharges waste heat from the electronics, and the latter rejects heat when the electric thrusters are not operating but power is still being produced. It was assumed that the PMAD radiator average temperature and areal density were 400 K and 7 kg/m<sup>2</sup>, respectively, while the parasitic load radiator values were 850 K and 10 kg/m<sup>2</sup>.

## IV. RESULTS

In this section, we present representative results from the mass models. The absolute values of alpha predicted are highly dependent on the assumptions made for component performance in the performance model, and on the various assumptions in the mass models. Because there is much hardware development to be done before these assumptions can be well-validated, the values of power system  $\alpha_{ps}$  predicted should not be taken to represent exactly what the  $\alpha_{ps}$  of a developed system will be. Rather, these plots are intended to show trends that illustrate parameters to optimize, and the relative contribution of the subsystems to  $\alpha_{ps}$ .

### IV.A. Areal Density

Fig. 5 shows the contribution of each of the radiator components to the areal density as a function of mass flow rate through the radiator. As discussed above, the ducting diameter need to increase to accommodate higher flow rates and soon becomes unreasonably large. For mass flow rates higher than 30 kg/s the ducting size is limited, and the additional fluid is assumed to be pumped through parallel loops. The vertical black lines represent the operating points for the 1200 K turbine inlet temperature cases discussed below. There is significant uncertainty in the mass of the pump due to low TRL of liquid metal pumps for this application, and the pump shown, or the triple loop case is very conservative estimate of the final mass. The triple loop configuration has a much lower mass flow rate due to the higher specific heat of NaK, less fluid is required to transfer the same energy. Fig. 5 shows that the triple loop is able to have a lower areal density. This is due to the lower mass flow rate as well as the much higher allowable pressure drop, as discussed in the next section.

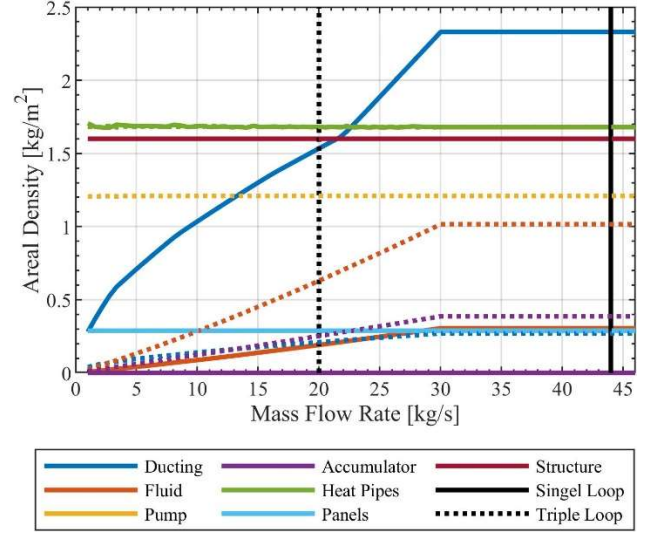


**Fig. 5.** Component areal densities, solid lines represent components in the single loop configuration and dashed lines represent components in the triple loop configuration

### IV.B. Optimization of Key Variables

#### IV.B.1. Radiator Pressure Drop

The radiator pressure drop is treated as an independent variable to be optimized. This is because the radiator pressure drop is the most important variable in determining the areal mass of the radiator. Fig. 6 shows  $\alpha_{ps}$  over a range of pressure drops for both loop configurations. A higher-pressure loss in the radiator results in smaller ducting and a lower radiator areal mass, but also decreases the cycle efficiency. This decrease in efficiency is much more pronounced in the single loop configuration where the compressor must account for the additional pressure loss. In the triple loop configuration, there is a separate pump in the radiator loop that can make up this pressure loss much more efficiently, resulting in a much higher optimal pressure loss and a lighter radiator.

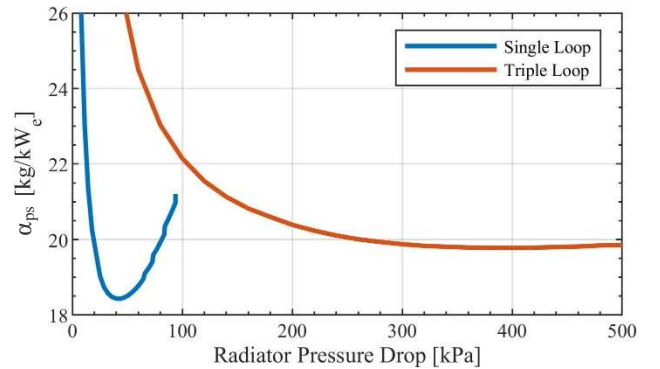


**Fig. 6.** Radiator pressure drop optimization

#### IV.B.2. Compressor Inlet Temperature

$\alpha_{ps}$  is also highly sensitive to the compressor inlet temperature. Fig. 7 shows the how  $\alpha_{ps}$  varies over a range

of compressor inlet temperatures for both loop configurations and a 1200 K and 1400 K turbine inlet temperature. A higher outlet temperature results in more radiative power per area, but a less efficient cycle. Due to radiative power being proportional to  $T^4$ , one might assume this effect would win out and drive the optimum to higher temperatures. This is the case when just the cycle thermodynamics are considered,<sup>3</sup> and the radiator area is optimized in Fig. 8. However, less efficient cycles will require more mass flow rate to reach the same power. This higher mass flow rate means that all the components will be larger. In particular, the ducting in the radiators will need to be larger and the areal density will increase for less efficient cycles. Due to this effect, the optimum  $\alpha$  occurs at a lower compressor inlet temperature than optimizing for radiator area using thermodynamics alone.

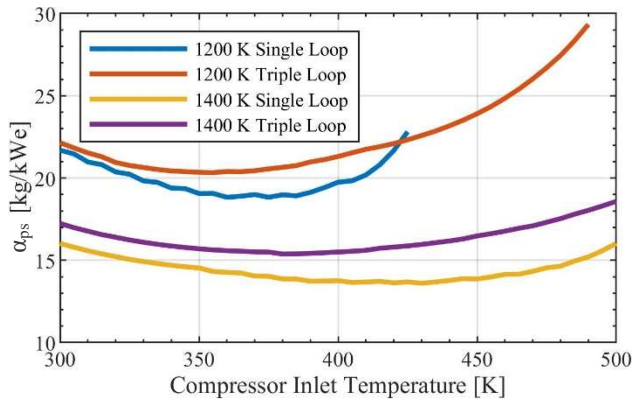


Fig. 7. Compressor inlet optimized with  $\alpha_{ps}$

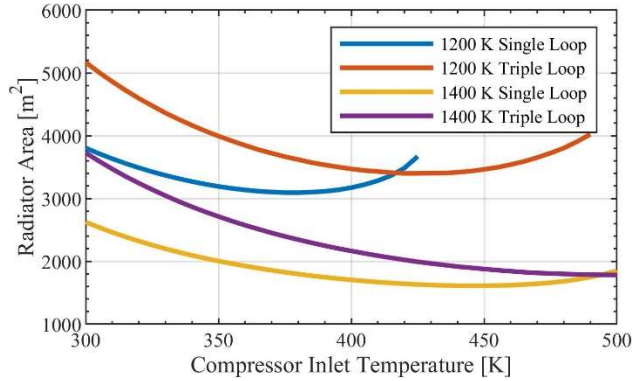


Fig. 8. Compressor inlet optimized with radiator area

#### IV.C. General Trends

Fig. 9 illustrates how  $\alpha_{ps}$  trends with increased power level. In this plot the optimum radiator pressure drops, and compressor inlet temperature are used. Generally,  $\alpha_{ps}$  is inversely related to power, but there are diminishing returns at higher power levels. It is also important to keep in mind that  $\alpha_{ps}$  is the specific mass and that the mass of the system will still increase with power. Fig. 9 shows that increasing the turbine inlet temperature results in much lower  $\alpha_{ps}$  for both loop configurations. A higher turbine

inlet temperature allows for both a higher efficiency and higher effective radiating temperature, which both drive the mass down.

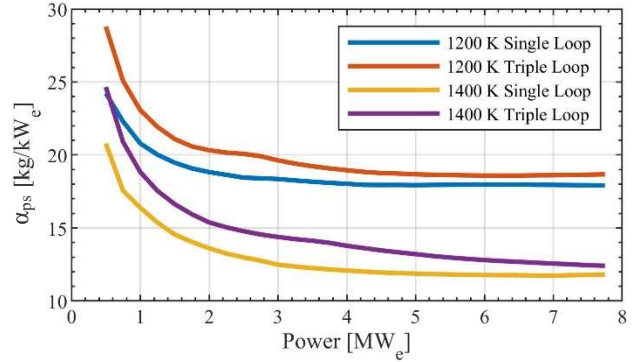


Fig. 9.  $\alpha_{ps}$  power scaling curves

Another observation is that the single loop configuration has a lower  $\alpha_{ps}$ . This difference is created by additional equipment in the separate loops including heat exchangers, pumps, and accumulators as well as the liquid metal working fluid being heavier than He-Xe gas. The triple loop configuration also has a slightly lower efficiency due to the temperature losses inherent in transferring energy across heat exchangers. Lower efficiency results in more waste heat and higher mass flow rates, which both increase  $\alpha_{ps}$ . These factors negate the slightly lighter radiators in the triple loop case from a higher allowable pressure drop. Fig. 10 shows the distribution of  $\alpha_{ps}$  between the different elements for representative points along the curve.

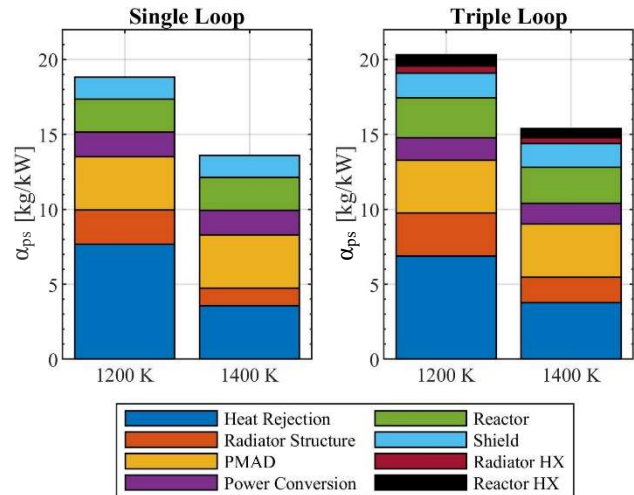


Fig. 10. Turbine inlet temperature effect on  $\alpha_{ps}$  for power level of 2 MW<sub>e</sub>

#### V. CONCLUSIONS

The heat rejection is by far the largest element of  $\alpha_{ps}$ . The radiator mass is reduced by increasing the radiator temperature or increasing the cycle efficiency. Unfortunately, these two approaches are in direct conflict

with each other and balancing them is central to NEP system design. Minimizing  $\alpha_{ps}$  is one way to balance these methods, and results in a lower optimal compressor inlet temperature than optimizing for radiator area does. Increasing the turbine inlet temperature, if possible, will allow improvement on both fronts and result in significant reduction in  $\alpha_{ps}$ .

Increasing power level will reduce  $\alpha_{ps}$ , but due to diminishing returns and a higher mass, this may not have benefits for a crewed Mars mission, where a minimal Earth departure mass is paramount. In some cases, electric propulsion thrusters with very high  $I_{sp}$ , such as MPD, optimize to a higher power level.<sup>4</sup> In these cases, the reduction in  $\alpha_{ps}$  achieved at high power levels may allow for a smaller Earth departure mass for crewed Mars mission using these thrusters.

From a purely mass perspective the single loop configuration outperforms the triple loop configuration. However, mass alone does not give a full picture of this trade. The triple loop configuration has several advantages over the single loop including: a more compact reactor, a more compact and more easily packed radiator, higher allowable radiator pressure drops, lower radiator areal mass, and potentially higher tolerance to micrometeoroid and orbital debris impacts. Developing a deeper understanding of these trades is the subject of future work.

The mass model presented here is intended to demonstrate trends within the design space, and not present exact numbers for a particular design point or prescribe a particular design choice. As the technology maturation effort continues and hardware is developed, better validation and assumptions will become available. These will allow for the model to be improved, and while the trends are expected to remain the same, the exact numbers and their relative magnitudes could change.

## ACKNOWLEDGMENTS

This work was supported by NASA's Space Technology Mission Directorate (STMD) through the Space Nuclear Propulsion (SNP) project. This work was funded under Contract No. 80LARC17C0003.

## REFERENCES

- [1] National Academies of Sciences, Engineering, and Medicine, "Space Nuclear Propulsion for Human Mars Exploration (2021)," *The National Academies Press*, Washington, DC, 2021.
- [2] M. Duchek, M. Clark, A. Pensado, C. Harnack, W. Macheimer, E. Grella and Qu, "Hybrid NEP-Chemical Vehicle and Propulsion Technology Study for Crewed Mars Missions," in *68th JANNAF Propulsion Meeting*, Virtual Event, 2021.
- [3] D. Nikitaev, D. C. Smith, M. Duchek, C. Harnack, W. Macheimer and G. Emanuel, "Nuclear Electric Propulsion Modular Power Conversion Model," in *Nuclear Emerging Technologies for Space*, Cleveland, OH, 2022.
- [4] M. Duchek, M. Clark and A. Pensado, "Sensitivity of Hybrid NEP-Chemical Vehicle Mass to Assumptions for Crewed Opposition-Class Mars Missions," in *AIAA Propulsion and Energy Forum*, Virtual Event, 2021.
- [5] A. C. Marshall, "RSMAS-D Models: An improved Method for Estimating Reactor and Shield Mass for Space Reactor Applications," Sandia National Laboratories, Albuquerque, 1997.
- [6] J. Holman, "Heat Transfer, 5th Edition," McGraw-Hill, 1981, pp. 210-211.
- [7] K. Polzin, To be published as *NEP Thermal Management Technical Interchange Meeting*, Space Technology Mission Directorate, 2021.
- [8] J.-M. Tournier and M. S. El-Genk, "Bellows-Type Accumulators for Liquid Metal Loops of Space Reactor Power Systems," The University of New Mexico, Albuquerque, NM, 2006.
- [9] J. E. Davis, "Design and Fabrication of the Brayton Rotating Unit," Airesearch Manufacturing Company of Arizona, Phoenix, 1972.
- [10] D. Nikitaev, C. D. Smith and K. Palomares, "Nuclear Thermal Propulsion Turbomachinery," in *Nuclear and Emerging Technologies for Space (NETS-2022)*, Cleveland, OH, 2022.
- [11] L. S. Mason, "A Power Conversion Concept for the Jupiter Icy Moons Orbiter," in *First International Energy Conversion Engineering Conference*, Portsmouth, 2003.
- [12] R. V. Boyle, W. J. B. Harper and C. T. Kudija, "Solar Dynamic CBC Power for Space Station Freedom," *American Society of Mechanical Engineers*, Brussels, Belgium, 1990.
- [13] B. Suden, "High Temperature Heat Exchangers (HTHE)," *Engineering Conferences International*, Hoboken, NJ, 2005.
- [14] J. Siamidis and L. S. Mason, "A Comparison of Coolant Options for Brayton Power Conversion Heat Rejection Systems," NASA Scientific and Technical Information Program Office, Langley, Virginia, 2006.
- [15] H. V. Chang, "Optimization of a Heat Pipe Radiator Design," in *ALAA 19th Thermophysics Conference*, Palo Alto, CA, 1984.
- [16] T. Kokan, R. Joyner, B. Reynolds, B. Muzek, D. Morris and R. Noble, "SNP Nexus EWG #10 NEP Update," 2020.
- [17] R. H. Frisbee and R. C. Moeller, "Identification of Mission Sensitivities for High-Power Electric Propulsion Systems," *41st AIAA/ASME/SAE/ASEE Joint Propulsion Conference and Exhibit*, 2005.